

# Interfacial reactions of Ti/*n*-GaN contacts at elevated temperature

C. J. Lu,<sup>a)</sup> A. V. Davydov,<sup>b)</sup> D. Josell, and L. A. Bendersky

*Materials Science and Engineering Laboratory, National Institute of Standards and Technology, Gaithersburg, Maryland 20899*

(Received 27 December 2002; accepted 11 April 2003)

Interfacial reactions in Ti/GaN contacts have been studied using conventional and high-resolution transmission electron microscopy (TEM), energy-filtered TEM (EFTEM), and x-ray diffraction. The thin film contacts were fabricated by evaporating Ti on *n*-GaN and subsequent rapid thermal annealing in argon. An x-ray result shows that the as-deposited Ti on GaN is an epitaxial hcp phase, whereas a fcc phase was identified from the as-deposited metal layer in cross-sectional TEM specimens. This phenomenon is interpreted as the transformation of hcp-Ti phase to fcc-TiH<sub>x</sub> phase by hydrogen incorporation during TEM specimen thinning. At elevated temperature, first gallium and then nitrogen diffused into the metal layer. The reaction front moved into the Ti layer, and after annealing at 700 °C many voids were formed along the Ti/GaN interface at the GaN side. A sequence of phases GaN/TiN/Ti<sub>2</sub>GaN/Ti<sub>3</sub>Ga/Ti was identified in annealed contacts, and corresponds to the expected diffusion path. The ternary phase Ti<sub>2</sub>GaN was confirmed with electron diffraction and EFTEM. A planar TiN layer, which formed in direct contact to the GaN, presumably governs the electrical properties of the alloyed contact. © 2003 American Institute of Physics. [DOI: 10.1063/1.1579128]

## I. INTRODUCTION

Current progress in the fabrication of nitride-based electronic and optical devices, such as visible light-emitting diodes and metal–semiconductor field-effect transistors, makes the formation of reliable metal contacts to GaN essential.<sup>1–3</sup> The development of thermally stable ohmic contacts to GaN is one of the main challenges for GaN-based device technology.<sup>1</sup> At elevated temperatures the onset of metal–GaN reactions can change the interface chemistry and morphology substantially, a general concern in the fabrication of Ga–N based devices. However, the nature of these metal/GaN interactions is not well understood.<sup>4</sup> It also remains unclear just how the changes in interface morphology and chemistry affect the electrical properties of the contact.

Many efforts to reduce the ohmic contact resistance of metal contacts on *n*-GaN epilayers have been reported recently.<sup>5–9</sup> The metallization schemes generally include Ti as the first metal layer. Smith *et al.*<sup>8</sup> reported that interfacial reactions between the Ti-based contacts and the *n*-GaN can beneficially affect the electrical properties of the contacts. In particular, studies have indicated that formation of a TiN layer may be important for ohmic contact development because of its low work function and the creation of nitrogen vacancies in the GaN below the contact layer when the Ti and GaN react.<sup>5,7–10</sup> Cordes and Chang<sup>11</sup> also identified the diffusion path of GaN/TiN/Ti<sub>2</sub>GaN/Ti<sub>3</sub>Ga/Ti at reacted Ti/GaN interfaces using diffusion couples, though the reaction mechanism was not clearly identified.

The present investigation focuses on the temperature-induced morphological and chemical changes of Ti/*n*-GaN

interface formation. X-ray diffraction (XRD) and various transmission electron microscopy (TEM) techniques, including selected area electron diffraction (SAED), energy-filtered TEM (EFTEM), and high-resolution electron microscopy (HRTEM), are used to obtain chemical and structural information from nanoscale interface areas.

## II. EXPERIMENT

Hydride vapor phase epitaxy (HVPE) grown *n*-GaN thin film on *c*-sapphire, supplied by Technologies and Devices International, Inc.,<sup>12</sup> was used for the Ti contact studies. Before being loaded into the vacuum system for metal deposition, the GaN surface was degreased sequentially in boiling chloroform, acetone, and methanol. The degrease was followed by an etch using a cold solution of HF:H<sub>2</sub>O (1:1) for 20 s. The etch was terminated using a boiling NH<sub>4</sub>OH:H<sub>2</sub>O<sub>2</sub>:H<sub>2</sub>O (1:1:3) bath followed by washing in boiling deionized water. Finally, the GaN surface was blown dry with nitrogen. A 22 nm thick Ti layer was deposited at room temperature by electron-beam evaporation. The base pressure of the chamber was  $9.3 \times 10^{-6}$  Pa and pressure was maintained below  $2.7 \times 10^{-5}$  Pa during deposition. After metallization, the material was cleaved into smaller samples. The samples were annealed in a rapid thermal annealing (RTA) furnace at temperatures between 400 and 700 °C for 30 s in flowing argon that had been freed of oxygen and water vapor using a titanium getter furnace.

XRD scans were collected at ambient temperature on a standard  $\theta$ - $2\theta$  diffractometer in symmetric reflection geometry using Cu  $K\alpha$  radiation. The cross-sectional slices for TEM investigation were obtained by cutting the Ti/GaN samples along the (11 $\bar{2}$ 0) plane of the GaN, gluing the cut pieces with the Ti coatings facing inward, and then thinning by mechanical grinding, polishing, dimpling, and Ar-ion

<sup>a)</sup>Present address: Department of Physics, Hubei University, Wuhan 430062, People's Republic of China

<sup>b)</sup>Electronic mail: davydov@nist.gov

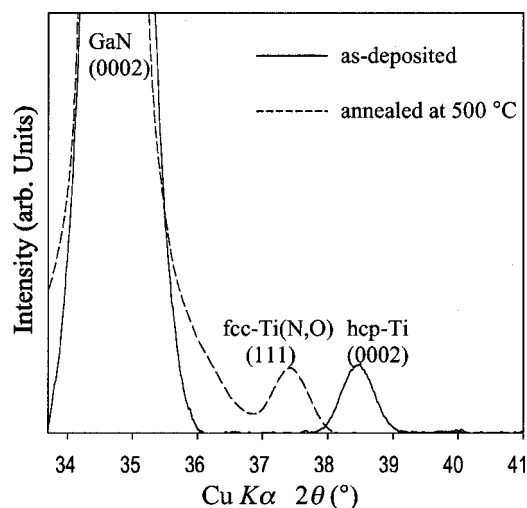


FIG. 1. XRD scans of Ti thin films on GaN/sapphire: (a) as-deposited and (b) annealed at 500 °C.

milling. The TEM investigations were carried out on a Philips EM430 microscope operated at 200 kV and on a JEOL3010 (300 kV) microscope with point-to-point resolution of 0.167 nm. High resolution and energy-filtered images were recorded on the JEOL 3010 with a slow-scan charge coupled device (CCD) camera. Elemental distribution maps of Ga, N, Ti, and O were acquired by energy filtered imaging using the three-window method.<sup>13</sup> The maximum scattering angle was determined by the objective lens aperture, yielding an acceptance half-angle  $\alpha = 4.5$  mrad and associated spatial resolution of 0.55 nm.

### III. RESULTS

#### A. As-deposited Ti film on GaN

Figure 1 shows an XRD scan of the as-deposited Ti and 500 °C annealed thin films on GaN/sapphire. Aside from the

(0002) GaN reflection at 34.65°, only a peak at  $2\theta = 38.46^\circ$  ( $d = 0.234$  nm) is seen for  $2\theta$  in the range 34°–41°. This peak corresponds to the (0002) reflection of the equilibrium hexagonal closed-packed (hcp) phase of bulk Ti (see Table I). Thus, as one might expect, the XRD results indicate that the Ti film deposits with an orientation (0002)hcp-Ti//((0002)GaN).

Interestingly, the x-ray result is inconsistent with most TEM observations; in the majority of cross-sectional TEM specimens, the Ti layer has a face-centered cubic (fcc) structure. Only a few TEM specimens exhibited the hcp-Ti phase indicated by the XRD results. Figure 2(a) shows a typical bright field TEM image of the cross-sectioned Ti film. Figure 2(b) is the SAED pattern from this area, taken along  $[1\bar{1}20]$  GaN. The GaN diffraction spots are indicated with an “X.” The remaining spots belong to the metal layer and index as two twin variants of an fcc phase viewed along the  $[\bar{1}10]$ . The two variants in the metal layer are visible as either dark or bright regions in Fig. 2(a). The measured spacings  $d_{111}$  and  $d_{002}$  for the fcc phase are about 0.255 and 0.221 nm, respectively.

The fcc crystal structure does not appear on the equilibrium, pressure-temperature phase diagram of bulk Ti.<sup>14</sup> Furthermore, the measured lattice constant of the fcc phase ( $a = 0.442$  nm) differs significantly from the 0.415 nm value obtained from strain analysis of quantitative low-energy electron-diffraction data for 2.5 nm thick Ti films on (001)Al as well as the 0.411 nm value theoretically calculated for fcc-Ti (see Table I).

The epitaxial growth of fcc-Ti thin films up to tens of nanometers thick has been reported on various substrates: NaCl single crystals,<sup>15</sup> (001)Ni,<sup>16</sup> and SiC semiconductor.<sup>17</sup> Face-centered-cubic Ti has also been reported to exist in ultrathin (less than 2 nm thick) Ti films deposited on (011)Al,<sup>18</sup> and (001)Al,<sup>19–21</sup> as well as in cross-sectional Ti/Ni and

TABLE I. Lattice spacings of possible interfacial phases (International Center for Diffraction Data).

Phase	Symmetry	Lattice constants (nm)	$d$ spacing (nm) ( $hkl$ )	
$\alpha$ -Ti	Hexagonal	$a = 0.295$	0.256 (10 $\bar{1}$ 0)	0.234 (0002)
	$P6_3/mmc$	$c = 0.469$		
$\gamma$ -Ti	Cubic	0.411	0.237 (111)	0.206 (200)
	$Fm\bar{3}m$	calculated <sup>a</sup>		
$\gamma$ -Ti	Cubic	0.415	0.240 (111)	0.208 (200)
	$Fm\bar{3}m$	measured <sup>b</sup>		
TiH <sub>2</sub>	Cubic	0.445	0.257 (111)	0.223 (200)
TiN	Cubic	0.424	0.245 (111)	0.212 (200)
	$Fm\bar{3}m$			
TiO	Cubic	0.418	0.241 (111)	0.209 (200)
	$Fm\bar{3}m$			
Ti <sub>3</sub> Ga	Hexagonal	$a = 0.574$	0.497 (10 $\bar{1}$ 0)	0.231 (0002)
	$P6_3/mmc$	$c = 0.463$		
Ti <sub>2</sub> GaN	Hexagonal	$a = 0.300$	0.260 (10 $\bar{1}$ 0)	0.666 (0002)
	$P6_3/mmc$	$c = 0.133$		
$\alpha$ -GaN	Hexagonal	$a = 0.319$	0.276 (10 $\bar{1}$ 0)	0.259 (0002)
	$P6_3mc$	$c = 0.518$		

<sup>a</sup>A. Aguayo, G. Murrieta, and R. de Coss, Phys. Rev. B **65**, 092106 (2002).

<sup>b</sup>Reference 19.

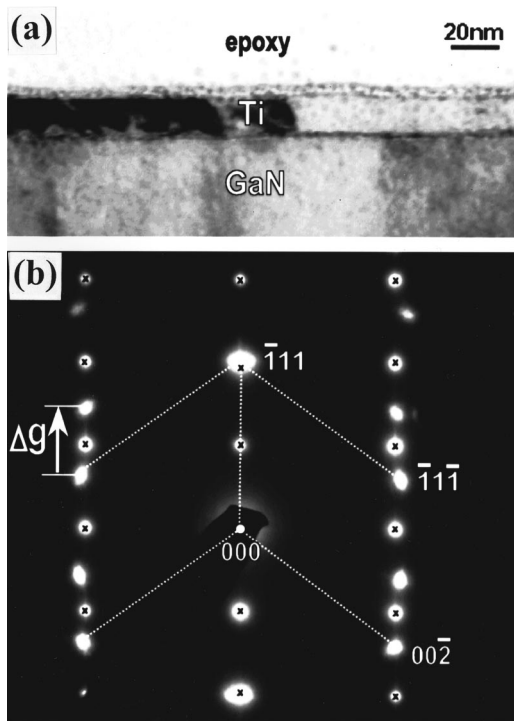


FIG. 2. (a) Bright field TEM image of the as-deposited Ti film on GaN, along with (b) the corresponding SAED pattern showing the combined patterns of  $[11\bar{2}0]\text{GaN}/[1\bar{1}0]\text{fcc-TiH}_x$ . All GaN spots are indicated with an "X." The fcc- $\text{TiH}_x$  exhibits two twin orientations on the GaN surface, and here one is indexed, and spots from the other are also present.

Ti/Al multilayers.<sup>16,22</sup> However, all the reports were based on TEM investigations; it was also demonstrated that fcc-Ti in Ti/Al, Ti/Ni, and Ti/Zr multilayers formed merely as an artifact of the specimen preparation for cross-sectional TEM.<sup>23–27</sup> Importantly, fcc phases exist for hydrides, nitrides, and oxides of Ti.<sup>28–32</sup> Elemental maps of the metal layer (not shown) eliminate the possibility of either an oxide (35–55 at. % O) or nitride (28–50 at. % N) phase aside from in the top 5 nm of the layer.<sup>28,29</sup> However, the inability to detect hydrogen in elemental maps by energy-filtered imaging means that a hydrogen-rich (51–67 at. % H) phase is a possibility.<sup>30–32</sup> Moreover, the measured spacings  $d_{111}$  and  $d_{002}$  for the fcc phase agree well with those of fcc- $\text{TiH}_2$  (see Table I), consistent with the presence of a fcc- $\text{TiH}_x$  ( $1 < x < 2$ ) phase in the cross-sectional TEM specimens.

The measured lattice parameter of the fcc-Ti material in Ti/Al multilayers was also reported to be 0.442 nm,<sup>23</sup> similar to that of fcc- $\text{TiH}_2$ , and suggesting hydrogen pickup as the source of the hcp to fcc transformation artifact in that case as well. Relevantly, the formation of fcc-based hydrides in thinned TEM specimens is well documented for Ti and Zr,<sup>33</sup> hydrogen stabilizes the fcc phase of Ti as an octahedral or tetrahedral interstitial.<sup>30,31</sup> In any case, the observation of the expected hcp-Ti phase peak in the XRD indicates that the fcc phase observed by TEM is merely an artifact of TEM specimen preparation. The hcp-Ti structure in Ti/Al multilayers has been stabilized in TEM cross sections when using ion mills with liquid nitrogen cooling and clean (oil-free) vacuum systems.<sup>34</sup> Therefore crystal structures determined

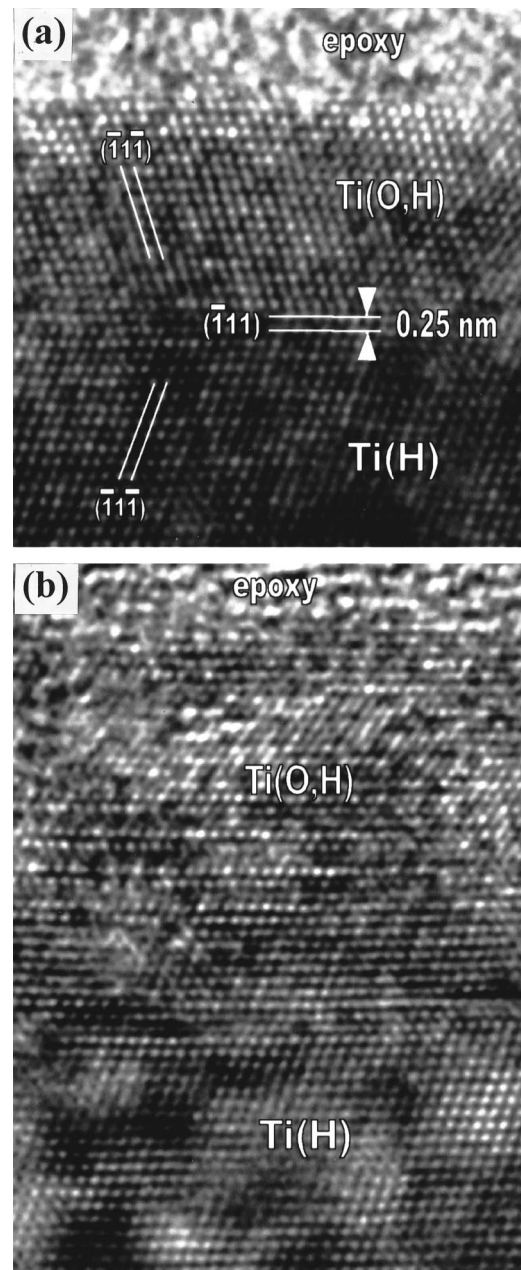


FIG. 3. Cross-sectional HRTEM images showing the surface layer of the as-deposited Ti film. The surface layer was contaminated by oxygen, probably in the form of water vapor. (a) A twin-like boundary was formed between fcc- $\text{Ti(H,O)}$  and fcc- $\text{TiH}_x$ , and (b) the surface layer shows three-layer repeat moiré fringes due to the overlapping of fcc- $\text{Ti(H,O)}$  grains having twin orientations.

by cross-sectional TEM are understood to require confirmation by another technique (e.g., XRD).

It is evident in Fig. 2(a) that a 5 nm thick surface layer of the Ti film exhibits different contrast than the remainder of the Ti layer. Energy-filtered imaging indicates the presence of oxygen in this region. The oxygen, probably in the form of water vapor, was likely adsorbed on the film surface when the specimen was exposed to air. Figure 3 shows two typical cross-sectional HRTEM images for the entire Ti layer. The image of Fig. 3(a) includes a twin boundary on the  $(\bar{1}11)$  plane, which is parallel to the Ti/GaN interface. Above the boundary the phase is  $\text{Ti(H,O)}$  and below the boundary it is

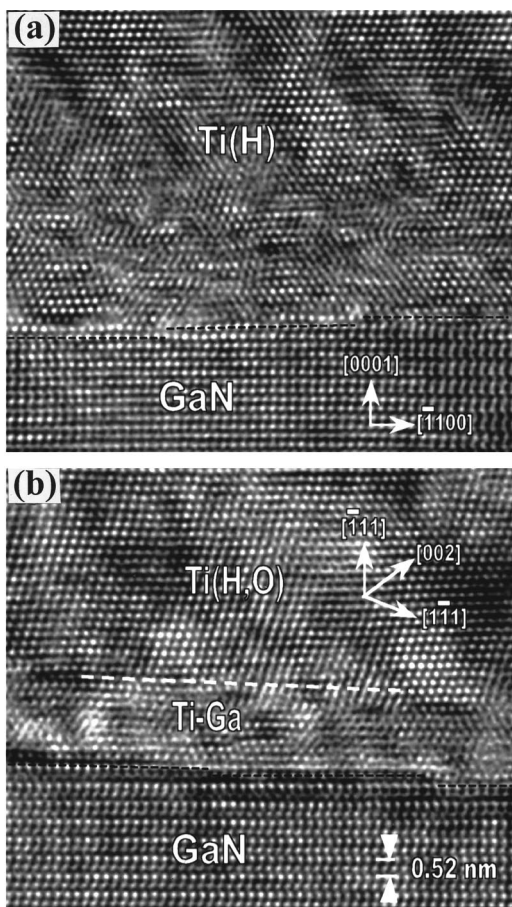


FIG. 4. HRTEM images showing (a) the Ti/GaN interface of the as-deposited film, and (b) the Ti/GaN interface after annealing at 400 °C.

TiH<sub>x</sub>. In Fig. 3(b) the top layer of the metal film shows enhancement of (111) fringes. The enhanced lattice fringes are moiré fringes due to overlapping twins; because the difference between the diffraction vector (002) of one twin and the vector ( $\bar{1}\bar{1}\bar{1}$ ) of another twin equals 1/3 the diffraction vector ( $\bar{1}\bar{1}\bar{1}$ ) of the two twins, i.e.,  $\Delta\mathbf{g}=(\mathbf{g}_{002})_{\text{twin1}} - (\mathbf{g}_{\bar{1}\bar{1}\bar{1}})_{\text{twin2}} = \frac{1}{3}\mathbf{g}_{\bar{1}\bar{1}\bar{1}}$  [see Fig. 2(b)], the moiré fringes exhibit a three-layer repeat contrast.

Figure 4(a) is a HRTEM image showing the Ti/GaN interface of the as-deposited specimen; steps along the Ti/GaN interface are indicated. Within the first 3 nm from the interface, the Ti layer contains numerous misfit dislocations and microtwins. One such small twin is located at the left side of the image. Energy-filtered chemical mapping indicates no chemical diffusion at the interface between the as-deposited Ti and GaN.

## B. Evolution of the Ti/GaN interface at elevated temperatures

According to XRD results (not shown), the Ti film still has an hcp structure after the 400 °C anneal. As with the as-deposited specimen, it was found that the annealed Ti film transformed to an fcc phase during TEM specimen preparation. Figure 4(b) is a cross-sectional HRTEM image of the Ti–GaN contact annealed at 400 °C; lattice planes for the fcc phase, presumably TiH<sub>x</sub>, are indicated on this [110] zone

axis image. EFTEM observations (not shown) indicate that gallium has diffused into a portion of the Ti layer, as indicated in Fig. 4(b). The complicated contrast in this region is probably related to the Ga alloying. No nitrogen was detected in the Ti layer though the elemental map of oxygen shows that a small amount of oxygen is distributed homogeneously over the entire metal layer. It is believed that the oxygen that was originally adsorbed on the top surface of the as-deposited Ti film diffused into the entire Ti layer during the 400 °C anneal.

EFTEM results (not shown) indicate that at 500 °C nitrogen started to diffuse into the metal layer following the diffusion of gallium. In the XRD scan of the Ti/GaN contact annealed at 500 °C (see Fig. 1), the (0002) reflection of hcp-Ti disappears and a new peak appears at  $2\theta = 37.33^\circ$  ( $d=0.241$  nm). Presuming that the new peak corresponds to the (111) reflection of an fcc-Ti phase, one obtains the lattice parameter  $a=0.417$  nm (see Table I); importantly, an fcc phase with this lattice parameter was also observed in cross-sectioned TEM specimens. The XRD and TEM results together indicate that the hcp phase has indeed transformed to the fcc structure during the 500 °C anneal. The fcc phase is not pure metal; it is stabilized by the presence of nitrogen and oxygen.

Figure 5 shows cross-sectional elemental maps of the Ti/GaN contact annealed at 600 °C, along with a bright field image of the contact structure. The N map (N-K edge at 394 eV) in Fig. 5(b) indicates nitrogen has diffused into the Ti layer to form a 5-nm-thick TiN<sub>y</sub> near-interface layer. Above the near-interface layer, a Ga-rich layer has formed, as shown in Fig. 5(d). A corresponding region of intermediate Ti content is visible in the Ti map of Fig. 5(c), suggesting that a Ti–Ga intermetallic compound layer has formed above the near-interface TiN<sub>y</sub> layer. The O map in Fig. 5(e) indicates that the top region of the Ti film is contaminated with oxygen while the oxygen content in the near-interface, nitrogen-rich region is much lower.

SAED and HRTEM were used to identify the interface phases. Figure 6(a) is a bright field image of the Ti/GaN contact annealed at 600 °C and the SAED pattern from this region is shown in Fig. 6(b). The GaN spots are indexed and indicated by an X in Fig. 6(b). Four spots around ( $1\bar{1}0$ )GaN are denoted by 1, 2, 3, and 4; the measured spacings for the spots are  $d_1=0.263$  nm,  $d_2=0.245$  nm,  $d_3=0.229$  nm, and  $d_4=0.211$  nm. The spacings  $d_2$  and  $d_4$  agree well with the  $d_{111}$  and  $d_{200}$  of TiN (see Table I). The spacing  $d_1$  is closest to the  $d_{1\bar{1}0}$  value of Ti<sub>2</sub>GaN while the value of  $d_3$  is close to the  $d_{200}$  of Ti<sub>3</sub>Ga (see Table I). Thus the SAED results suggest the formation of TiN, Ti<sub>2</sub>GaN, and Ti<sub>3</sub>Ga in the contact structure. Figure 7 shows a lattice image of the near-interface region of the contact annealed at 600 °C, taken along the direction of  $[11\bar{2}]$ GaN. In the first 5 nm adjacent to the GaN surface one can see three-layer repeat contrasts indicated by arrows. These moiré fringes are frequently seen due to the overlapping of nanoscale fcc-TiN grains having twin orientations [as per the discussion for fcc-Ti(O) twins in Sec. III A]. Above the first 5 nm the lattice images are irregular, suggesting the presence of very small Ti–Ga and Ti<sub>2</sub>GaN grains as well as fcc-Ti(N) or Ti(O,N).

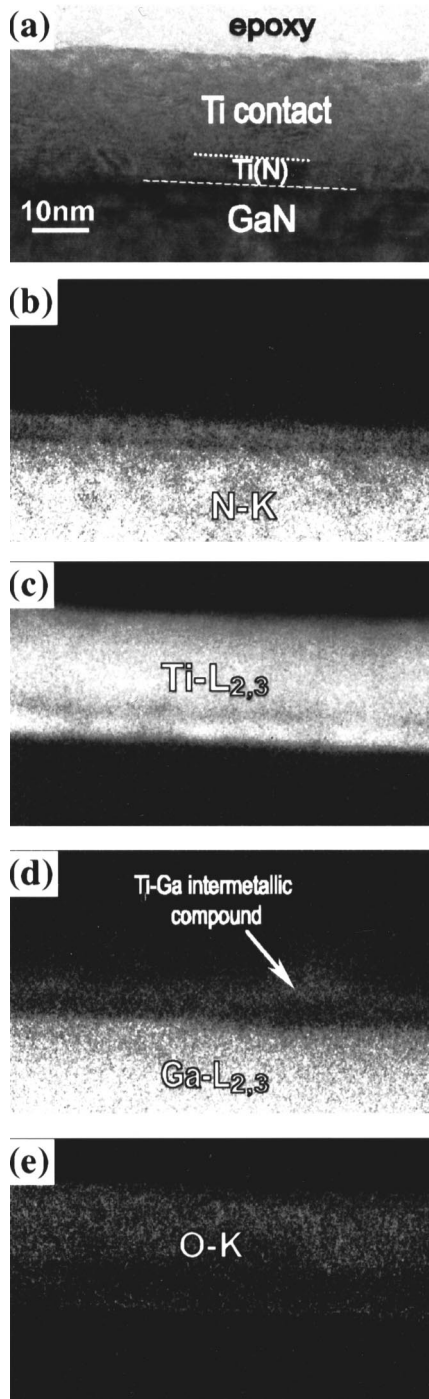


FIG. 5. Cross-sectional EFTEM images of the Ti/GaN contact annealed at 600 °C: (a) bright-field image of the contact structure; (b)–(e) elemental distribution maps of the elements N, Ti, Ga, and O for the same area in (a).

Growth of the TiN grains was observed in the specimens annealed at 700 °C. Figure 8(a) shows the lattice image of a large TiN grain in a [110] orientation. The interplane spacings of the grain are measured to be  $d_{111}=0.244$  nm and  $d_{002}=0.210$  nm, in good agreement with values for TiN (see Table I). More significantly, while the Ti/GaN interface was still flat and sharp after annealing at 600 °C [Figs. 6(a) and 7], the interface geometry changed substantially when it was annealed at 700 °C; numerous nanoscale voids formed in the GaN just under the interface.

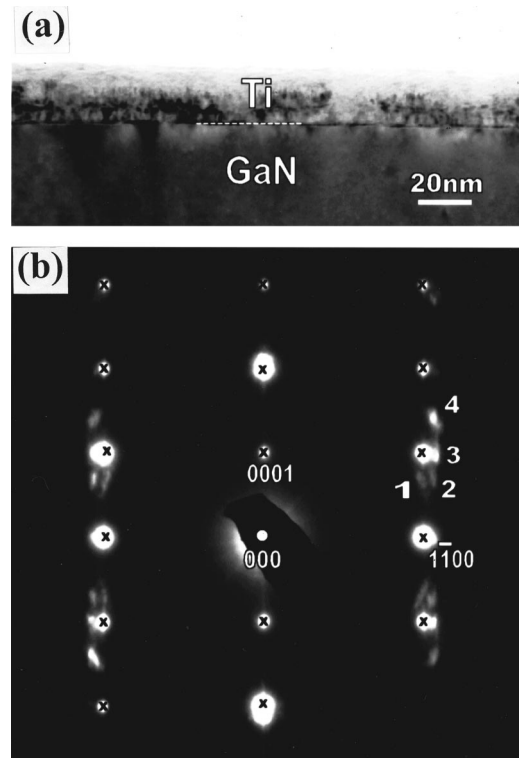


FIG. 6. (a) Bright-field TEM image of the Ti/GaN contacts annealed at 600 °C, along with (b) the SAED pattern from the region. The GaN spots are indicated by an “X” and are indexed. (b) The combined patterns of  $[11\bar{2}0]$ GaN// $[1\bar{1}0]$ Ti(N,O)// $[11\bar{2}0]$ Ti<sub>2</sub>GaN + Ti<sub>3</sub>Ga.

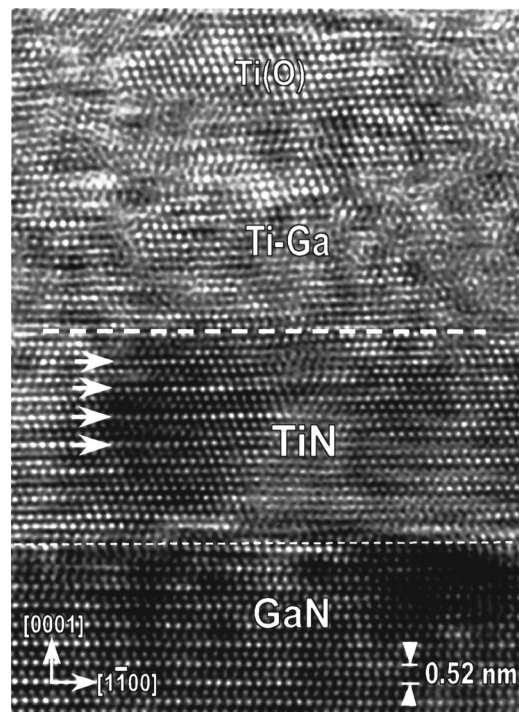


FIG. 7. HRTEM image showing the TiN interface layer of the contact annealed at 600 °C. The three-layer repeat contrast indicated by arrows are moiré fringes due to the overlapping of fcc-TiN grains having twin orientations.

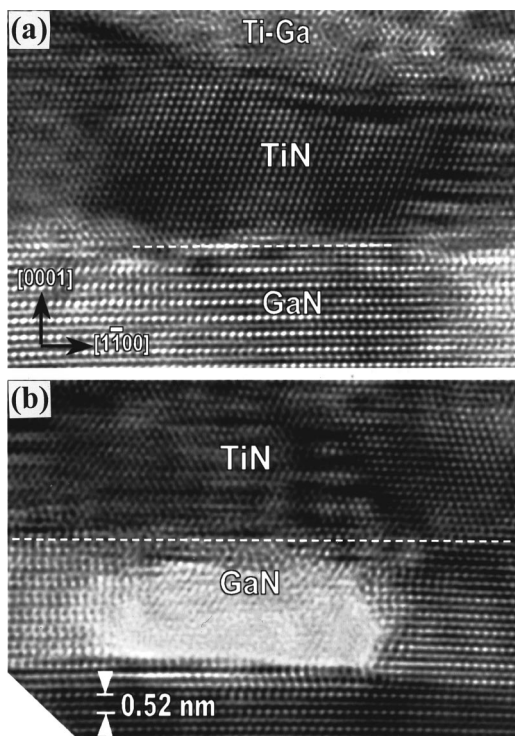


FIG. 8. HRTEM images showing the near-interface structure of the contact annealed at 700 °C. (a) A large TiN grain was identified at the interface, and (b) another region including a void just under the interface, which is indicated with a dashed line.

indicated in a bright field image [see Fig. 9(a)] of the Ti/GaN contact annealed at 700 °C. An HRTEM image of one void is shown in Fig. 8(b). The SAED pattern from the region shown in Fig. 9(a) is shown in Fig. 9(b); it is the combined patterns of  $[11\bar{2}0]\text{GaN}/[110]\text{TiO}_z/[110]\text{TiN}_y$ . The measured spacings of  $d_{111}=0.242$  nm and  $d_{002}=0.210$  nm are close to those of TiO and TiN (see Table I). Thus, SAED and HRTEM results suggest the presence of  $\text{TiO}_z$  and  $\text{TiN}_y$  in the contact annealed at 700 °C, confirmed by EFTEM observations. Figure 10(a) shows a bright-field image of the Ti/GaN contact annealed at 700 °C and Figs. 10(b)–10(e) are the elemental distribution maps of the elements N, Ti, Ga, and O for the same region in Fig. 10(a). This region includes two voids denoted by 1 and 2 which appear as dark regions in all the elemental maps. Above the voids is a very thin (less than 2 nm) layer containing Ti, Ga, and N, followed by a 4 nm thick TiN layer [see Figs. 10(b)–10(d) near the interface]. Above the TiN layer is a Ti–Ga layer 5 nm thick. In this layer, some regions are Ti-rich while others are Ga-rich [see Figs. 10(c) and 10(d)]. One can see from Fig. 10(e) that the near-interface TiN layer contains much less oxygen than the region immediately above it. Figure 10(f) shows an electron energy loss spectrometry (EELS) spectrum acquired from the small area circled in Fig. 10(a). It can be estimated that the content of oxygen in the top layer is less than 20 at. %. Therefore the top layer is an fcc-Ti(O) phase in the TEM specimen.

#### IV. DISCUSSION

All XRD and TEM analyses are summarized in Table II. The as-deposited Ti film has an hcp structure and grew epi-

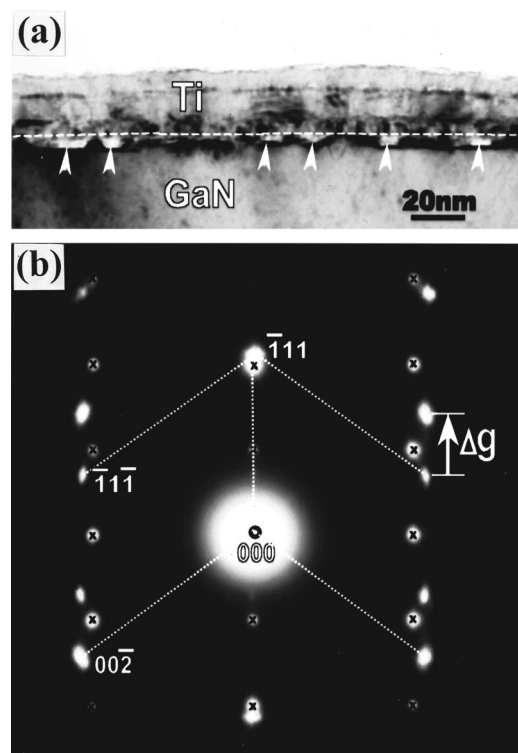


FIG. 9. (a) Bright-field TEM image of the Ti/GaN contacts annealed at 700 °C, along with (b) the SAED pattern from the region. (b) The combined patterns of  $[11\bar{2}0]\text{GaN}/[1\bar{1}0]\text{Ti(N,O)}$ . All GaN spots are indicated by an “X” and the spots of fcc-Ti(N,O) are indexed. In (a) the interface is indicated by a dashed line while voids under the interface are marked with arrowheads.

taxially on the GaN. After annealing at 500 °C for 30 s in Ar, the film transformed into an fcc structure. This fcc-Ti phase is believed to be stabilized by a small amount of nitrogen, which has begun to diffuse into the Ti at this temperature. It has been reported that the early nitriding stage of evaporated-Ti thin films by N-ion implantation is accompanied by the transformation of hcp-Ti to  $\text{TiN}_y$  ( $y$  could be  $<0.027$ ) with an fcc-Ti sublattice.<sup>35</sup> The same group reported that the implantation of N can dissociate H from fcc- $\text{TiH}_x$ . Both those results are consistent with the crystal structure change after the 500 °C anneal indicated here by XRD (Fig. 1), the displacement of oxygen by nitrogen at 600 °C indicated here by EFTEM (Fig. 5), and elimination of the fcc- $\text{TiH}_x$  artifact phase in the TEM specimens of contacts after anneals at 500 °C and above.

In this study, a planar TiN layer formed in direct contact to the GaN after annealing at 600 °C. This is consistent with a previous report that a thin TiN layer was observed by TEM even in as-deposited Ti contacts on GaN substrate treated by reactive ion etching,<sup>10</sup> although no evidence of a TiN layer was found in the as-deposited Ti/GaN in this study by either XRD or high-resolution EFTEM. A transformation of the hcp-Ti on GaN to fcc- $\text{TiH}_x$  during TEM specimen thinning was observed; it was, however, merely an artifact of TEM specimen preparation. Careful analysis of both XRD and TEM results was necessary to avoid confusion, particularly in light of the presence of fcc phases including the artifact fcc- $\text{TiH}_x$  as well as the actual fcc-TiN and other phases. Use

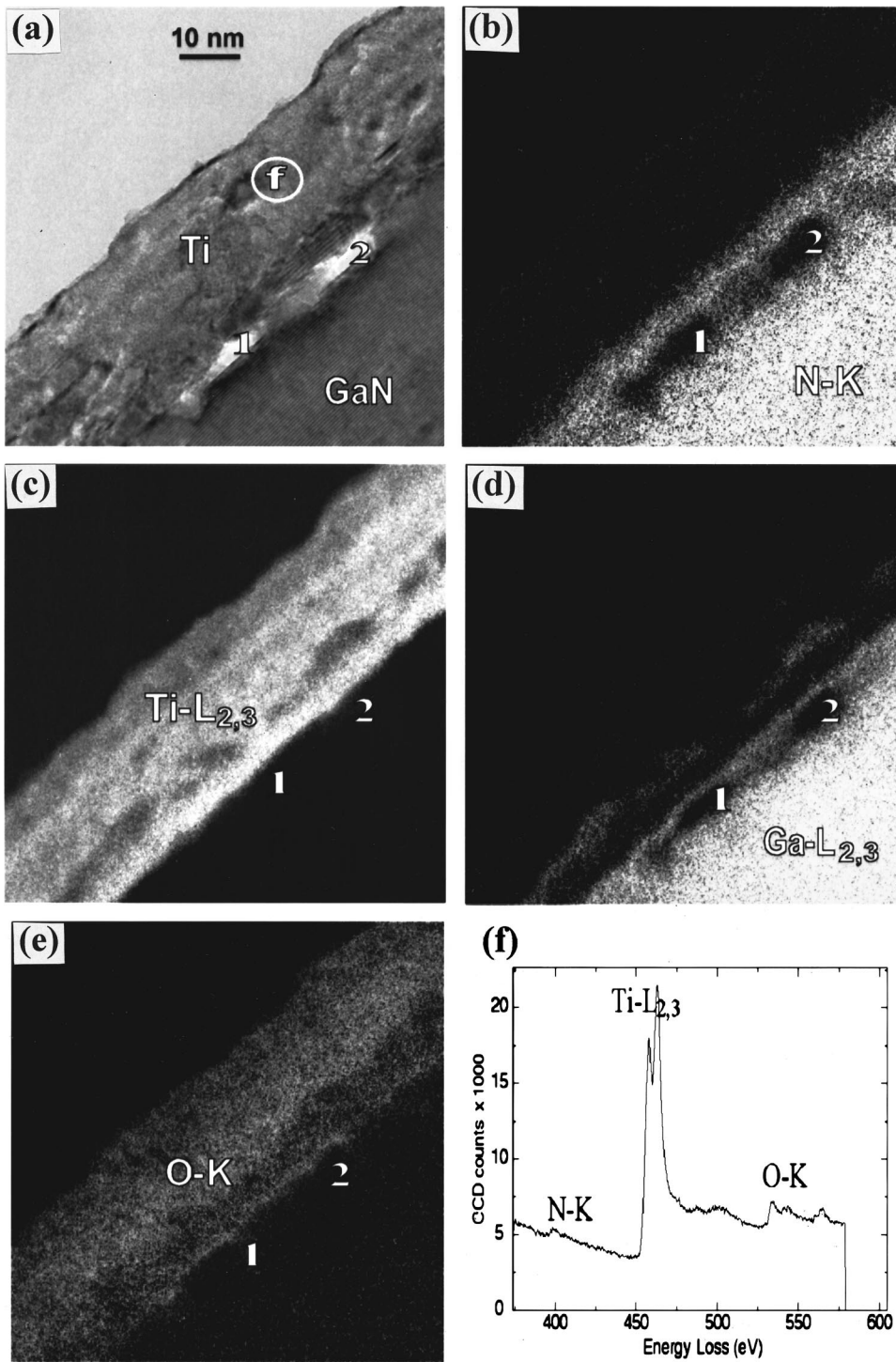


FIG. 10. (a) Bright-field TEM image of the Ti/GaN contact annealed at 700 °C, taken along the zone axis of  $[11\bar{2}0]$ GaN; (b)–(e) elemental distribution maps of the elements N, Ti, Ga, and O for the same region in (a). (f) EELS spectrum acquired from the small area circled in (a). Two voids under the interface are indicated with 1 and 2.

of liquid-nitrogen cooling and clean vacuum systems would help to stabilize the hcp-Ti structure during TEM specimen ion-milling.

The diffusion path:  $\text{GaN} \rightarrow \text{TiN} \rightarrow \text{Ti}_2\text{GaN} \rightarrow \text{Ti}_3\text{Ga} \rightarrow \text{Ti(N)}$  has been previously identified using the Ti–Ga–N phase diagram and interfacial analysis in bulk diffusion couples of Ti(foil)/GaN(pressed power) after 850 °C annealing for prolonged time.<sup>11</sup> This study of thin film Ti/GaN structures has identified a similar phase formation sequence in a series of 30 s anneals at temperatures between 400 and 700 °C. The results obtained here are also consistent with

those obtained by x-ray photoelectron spectroscopy depth profiling of chemical diffusion between a Ti thin film and GaN.<sup>9</sup> Depth profiles of gallium visible above an interface layer with a composition consistent with TiN, after annealing at 700 °C for 25 min in Ar, are qualitatively consistent with the TEM observations shown here.

In the observed interfacial layer sequence, the formation of a TiN phase is likely very important. TiN has a NaCl-type structure and has a reasonably close lattice match to hexagonal GaN (–5.9%) in the closed-packed  $\{111\}$  planes. Con-

TABLE II. Summary of the XRD and TEM results.

Annealing temperature	XRD	TEM phases and morphology	EFTEM and EELS
As-deposited	hcp-Ti	fcc-TiH <sub>x</sub> with twins or hcp-Ti	O at surface layer
400 °C	hcp-Ti(O)	fcc-TiH <sub>x</sub> (O) with twins	O in whole layer, Ga started to diffuse into the Ti layer
500 °C	fcc-Ti(N,O)	fcc-Ti(N,O)	N started to diffuse into the metal layer
600 °C		TiN/Ti <sub>2</sub> GaN/Ti <sub>3</sub> Ga, TiN next to GaN	Ti–Ga alloy above TiN
700 °C		TiN/Ti–Ga, Voids under interface	Heterogeneity in Ti–Ga layer

sistently, it was found in this study that TiN produced via the reaction of Ti with GaN, tended to orient its {111} planes with the GaN basal plane. The TiN layer was also found to be thermally stable and to inhibit oxidation from 500 to 700 °C.

TiN is thermodynamically stable in contact with GaN and most likely governs the electrical properties of the alloyed contact.<sup>36</sup> Both Ti and TiN are low work function metals, though TiN has the lower value ( $\phi_{\text{Ti}}=4.1$  eV,  $\phi_{\text{TiN}}=3.74$  eV). Thus, according to the Schottky–Mott–Bardeen model, TiN should more readily form ohmic contacts to *n*-type semiconductors. Furthermore, the reaction of Ti with GaN results in the formation of N vacancies in the GaN layer,<sup>5</sup> which function as shallow donors and promote higher conductivity of the Ti/GaN contacts.

During formation of the reaction phases, the reaction front moved toward the Ti layer, as determined by the presence of voids on the GaN side after annealing at 700 °C [Figs. 6(c), 8(b), and 9]. Specifically, it is diffusion of both the nitrogen and the gallium from the GaN into the Ti layer that produces the voids. Such voids would clearly be detrimental to the electrical properties of GaN devices. Annealing schedules for formation of the ohmic contacts must be appropriately designed to avoid such void formation.

## V. CONCLUSIONS

Various TEM techniques and XRD were employed to study the interfacial reactions in Ti/GaN contacts fabricated by evaporating Ti on HVPE-grown *n*-GaN followed by rapid thermal annealing in argon. The as-deposited metal layer on GaN is an epitaxial Ti thin film of hcp structure; it can transform from hcp-Ti to fcc-TiH<sub>x</sub> by hydrogen pickup as an artifact of cross-sectional TEM specimen thinning. The diffusion path of GaN/TiN/Ti<sub>2</sub>GaN/Ti<sub>3</sub>Ga/Ti is identified in the contacts annealed at 600 °C. A ternary phase Ti<sub>2</sub>GaN was confirmed by SAED and EFTEM. A planar TiN layer was formed in direct contact to GaN, which likely governs the electrical properties of the alloyed contact. As a result of gallium and nitrogen diffusing out from the GaN layer, the reaction front moved toward the Ti layer and after annealing at 700 °C numerous voids formed along the Ti/GaN interface at the GaN side.

## ACKNOWLEDGMENTS

The authors wish to thank D. Tsvetkov (Technologies and Devices International, Inc.) for providing GaN/sapphire sample, A. Motayed (Howard University, DC) for RTA pro-

cessing, S. W. Claggett and R. L. Parke of NIST for TEM specimen preparation, and J. E. Bonevich (NIST) for helpful discussions.

- <sup>1</sup>G. Popovici, H. Morkoc, and S. N. Mohammad, Group III Nitride Semiconductor Compounds, edited by B. Gil (Clarendon, Oxford, 1998), pp. 19–69.
- <sup>2</sup>A. Barinov, L. Casalis, L. Gregoratti, and M. Kiskinova, Phys. Rev. B **63**, 085308 (2001).
- <sup>3</sup>M. A. Khan, J. N. Kuznia, A. R. Bhattarai, and D. T. Olson, Appl. Phys. Lett. **62**, 1786 (1993).
- <sup>4</sup>A. N. Bright and C. J. Humphreys, Philos. Mag. B **81**, 1725 (2001).
- <sup>5</sup>M. E. Lin, Z. Ma, F. Y. Huang, Z. F. Fan, L. H. Allen, and H. Morkoc, Appl. Phys. Lett. **64**, 1003 (1994).
- <sup>6</sup>M. W. Fay, G. Moldovan, P. D. Brown, I. Harrison, J. C. Birbeck, B. T. Hughes, M. J. Uren, and T. Martin, J. Appl. Phys. **92**, 94 (2002).
- <sup>7</sup>S. H. Lim, W. Swider, J. Washburn, and Z. Liliental-Weber, J. Appl. Phys. **88**, 6364 (2000).
- <sup>8</sup>L. L. Smith, R. F. Davis, R. J. Liu, M. J. Kim, and R. W. Carpenter, J. Mater. Res. **14**, 1032 (1999).
- <sup>9</sup>B. P. Luther, S. E. Mohny, and T. N. Jackson, Semicond. Sci. Technol. **13**, 1322 (1998).
- <sup>10</sup>S. Ruvimov, Z. Liliental-Weber, J. Washburn, K. J. Duxstad, E. E. Haller, Z. F. Fan, S. N. Mohammad, W. Kim, A. E. Botchkarev, and H. Morkoc, Appl. Phys. Lett. **69**, 1556 (1996).
- <sup>11</sup>H. Cordes and Y. A. Chang, MRS Internet J. Nitride Semicond. Res. **2**, 2 (1997).
- <sup>12</sup>Certain commercial equipment, instruments, or materials are identified in this article in order to specify the experimental procedure adequately. Such identification is not intended to imply recommendation or endorsement by the National Institute of Standards and Technology, nor is it intended to imply that the materials or equipment identified are necessarily the best available for the purpose.
- <sup>13</sup>C. Jeanguillaume and C. Colliex, Ultramicroscopy **28**, 252 (1989).
- <sup>14</sup>D. A. Young, Phase Diagrams of the Elements (University of California, Berkeley, 1991).
- <sup>15</sup>F. E. Wawner Jr. and K. R. Lawless, J. Vac. Sci. Technol. **6**, 588 (1969).
- <sup>16</sup>A. F. Jankowski and M. A. Wall, J. Mater. Res. **9**, 31 (1994).
- <sup>17</sup>Y. Sugawara, N. Shibata, S. Hara, and Y. Ikuhara, J. Mater. Res. **15**, 2121 (2000).
- <sup>18</sup>A. A. Saleh, V. Shutthanandan, and R. J. Smith, Phys. Rev. B **49**, 4908 (1994).
- <sup>19</sup>S. K. Kim, F. Jona, and P. M. Marcus, J. Phys.: Condens. Matter **8**, 25 (1996).
- <sup>20</sup>P. M. Marcus and F. Jona, J. Phys.: Condens. Matter **9**, 6241 (1997).
- <sup>21</sup>A. A. Saleh, V. Shutthanandan, N. R. Shivaparan, R. J. Smith, T. T. Tran, and S. A. Chambers, Phys. Rev. B **56**, 9841 (1997).
- <sup>22</sup>R. Banerjee, R. Ahuja, and H. L. Fraser, Phys. Rev. Lett. **76**, 3778 (1996).
- <sup>23</sup>D. Shechtman, D. van Heerden, and D. Josell, Mater. Lett. **20**, 329 (1994).
- <sup>24</sup>D. Josell, D. Shechtman, and D. van Heerden, Mater. Lett. **22**, 275 (1995).
- <sup>25</sup>J. Bonevich, D. van Heerden, and D. Josell, J. Mater. Res. **14**, 1977 (1999).
- <sup>26</sup>J. Bonevich and D. Josell, Phys. Rev. Lett. **82**, 2002 (1999).
- <sup>27</sup>T. Tepper, D. Shechtman, D. van Heerden, and D. Josell, Mater. Lett. **35**, 100 (1998).
- <sup>28</sup>J. L. Murray and H. A. Wriedt, in Binary Alloy Phase Diagrams, edited by

- T. B. Massalski (ASM, Metals Park, OH, 1986), Vol. 1-2, pp. 1789, 1793, and 1794.
- <sup>29</sup>H. A. Wriedt and J. L. Murray, in Binary Alloy Phase Diagrams, edited by T. B. Massalski (ASM, Metals Park, OH, 1986), Vol. 1-2, pp. 1652, 1655, and 1656.
- <sup>30</sup>P. Dantzer, *J. Phys. Chem. Solids* **44**, 913 (1983).
- <sup>31</sup>R. Hempelmann, D. Richter, and B. Stritzker, *J. Phys. F: Met. Phys.* **12**, 79 (1982).
- <sup>32</sup>H. Numakura and M. Koiwa, *Acta Metall.* **32**, 1799 (1984).
- <sup>33</sup>J. C. Carpenter, J. A. Jackman, J. P. McCaffrey, and R. Alani, *J. Microsc. Soc. Am.* **4**, 175 (1995).
- <sup>34</sup>J. E. Bonevich (private communication).
- <sup>35</sup>Y. Kasukabe, S. Takeda, Y. Fujiwara, Y. Yamada, S. Nagata, M. Kishimoto, and S. Yamaguchi, *J. Vac. Sci. Technol. A* **15**, 1848 (1997).
- <sup>36</sup>S. E. Mohnney and X. Lin, *J. Electron. Mater.* **25**, 811 (1996).